Journal of Applied Physics ARTICLE pubs.aip.org/aip/jap

Revised identification of Ag-related defects in silver-doped Si by deep-level transient spectroscopy

Cite as: J. Appl. Phys. **138**, 175106 (2025); doi: 10.1063/5.0297836
Submitted: 21 August 2025 · Accepted: 20 October 2025 ·
Published Online: 4 November 2025

K. Gwozdz[1] and Vl. Kolkovsky[2,a)]

AFFILIATIONS

[1]Department of Experimental Physics, Faculty of Fundamental Problems of Technology, Wroclaw University of Science and Technology, Wybrzeze Wyspianskiego 27, Wroclaw 50-370, Poland
[2]Fraunhofer IPMS, Maria-Reiche St. 2, Dresden 01109, Germany

[a)]**Author to whom correspondence should be addressed:** uladzimir.kalkouski@ipms.fraunhofer.de

ABSTRACT

In the present study, we re-examine the electronic levels of silver-related defects in Si by deep-level transient spectroscopy (DLTS) and Laplace DLTS. We show that dominant Ag-related defects previously assigned to substitutional Ag could be only observed after annealing at 700 °C in our samples, and their appearance strongly depends on doping and post-annealing treatments conditions. The hydrogenation of the annealed Si samples leads to the appearance of several AgH-related defects. By analyzing the depth profiles of the defects, we attribute them to AgH-related complexes with one and two H atoms. From the analysis of the capture cross section and the electric field dependence, the charge state of the defects is also determined. We discuss the origin of the defects.

I. INTRODUCTION

Silicon is the foundational material in the semiconductor industry, playing a crucial role in the fabrication of various electronic devices, including transistors, diodes, and integrated circuits. Defects unintentionally introduced in silicon during the semiconductor fabrication process can significantly affect its electrical and optical properties. Among these defects, transition metals, particularly noble metals, are of special interest, as many of them can reduce the lifetime of minority carriers in silicon and lead to severe contamination of various tools in modern cleanrooms, especially those used in the production of diverse products. In this study, we focus on the investigation of silver and silver–hydrogen-related complexes in silicon. In microelectronics, silver is used as an interconnect material in integrated circuits, linking different components on a chip to facilitate data flow, and the incorporation of hydrogen is nearly unavoidable during device processing.

Due to their similar electron configurations, both having a filled *d*-subshell (d^{10}) and a single electron in the *s*-orbital, silver (Ag) is expected to exhibit chemical and physical properties similar to those of gold (Au), which has been extensively investigated in the literature.[1–7] Like Au, two dominant deep-level traps of Ag have also been reported in n- and p-type Si.[8–12] By analogy to Au, these levels were attributed to the single acceptor and single donor levels of substitutional Ag. However, solid evidence for this assignment is still lacking in the literature. Moreover, the dominant Ag levels observed in different studies show significant variation in their positions, ranging from 0.29 to 0.41 eV above the valence band for the single donor level, and from 0.5 to 0.6 eV below the conduction band for the single acceptor level.[8–12] The origin of this variation is unclear, and it cannot be explained by an enhancement of the emission rate of the defects in different electric fields.

Due to its similarities with Au^0 and taking into account the results of calculations reported in Ref. 13, a paramagnetic state of isolated substitutional Ag is also expected to be observed in Si. However, no electron paramagnetic resonance (EPR) spectra confirming the existence of a paramagnetic state for Ag have been reported in the literature. In contrast, Son *et al.*[14] observed an EPR signal related to isolated interstitial Ag atoms in samples doped with Ag by annealing at 1250 °C followed by quenching in water at room temperature, as well as several other Ag-related complexes. It appears that the formation of Ag_S depends on the conditions of Ag introduction and quenching parameters. In our preliminary study,[15] we showed that dominant Ag levels similar to those,

previously correlated with Ag_S (−/0) and Ag_S (0/+), could not be always observed in as-doped Si samples, and additional annealing steps are necessary to form these defects. The absence of the additional annealing steps after the introduction of Ag in Si may explain the absence of Ag_S in Ref. 14. In addition to Ag_S (−/0) and Ag_S (0/+), other Ag-related defects could also appear in samples doped with silver during the floating-zone growth process.[9,10] The concentration of these defects varies with the amount of Ag introduced during the growth. It also depends on the introduction conditions of Ag including the cooling rate of the samples[9,10,15] and on additional heat treatments performed for the activation of Ag defects.[15] Several of the Ag-related defects were assigned to an Ag–Ag pair or to an Fe–Ag complex.[9] The origin of other defects is still under discussion.

The interaction of hydrogen with Ag has also been extensively investigated in the literature, with several AgH-related defects reported in various studies.[9,15–17] Based on deep-level transient spectroscopy (DLTS) measurements and depth profile analyses of AgH-related defects, Yarykin *et al.*[10] proposed a schematic diagram for AgH complexes with one and two H atoms. However, different depth profiles near the surface were observed for defects attributed to different charge states of AgH with one H atom (E2 and E3). This observation is inconsistent with assigning E2 and E3 to different charge states of the same defect, although the author suggested the existence of another AgH-related defect near E2 that could not be resolved by conventional DLTS measurements and might account for the differences in the depth profiles. Using high-resolution Laplace DLTS,[18] we confirmed that the depth profiles of E2 and E3 are not identical near the surface, and we found no evidence of another complex defect in the vicinity of E2.[15]

It is worth noting that even after annealing at 500 °C in our preliminary study, several Ag-related complex defects can still be observed in both n- and p-type Si. These defects may interact with hydrogen, leading to the appearance of additional DLTS peaks and potentially resulting in misinterpretations of Ag_SH-related defects. Therefore, in this study, we annealed the as-doped samples at higher temperatures (around 700 °C) to eliminate complex defects before hydrogenating the annealed samples using wet chemical etching to investigate the interaction of Ag with H. We will show that under these conditions, a single dominant DLTS peak associated with Ag can be observed in both n- and p-type Si, which simplifies the study of AgH-related defects. By using Laplace DLTS measurements to determine the depth profiles of Ag and AgH-related defects and analyzing the electric field dependence of their emission rates, we discuss their origin.

II. EXPERIMENTAL

We employed float-zone Si samples doped with either P or B as shallow dopants, with concentrations ranging from 1×10^{14} to 2×10^{14} cm^{-3}. 15 mg of silver was introduced during crystal growth. After detaching the crystal, heating was immediately stopped, but the cooling rate was not consistent. The as-grown samples were polished using wet chemical etching (WCE) in CP4A ($HF:HNO_3:CH_3COOH$ 3:5:3) at room temperature. Hydrogenation of the Ag-doped samples resulted in the emergence of several DLTS peaks, which are not the focus of this study. To eliminate these defects, the samples were annealed at various temperatures ranging from 500 to 700 °C for 60 min before the preparation of Schottky and Ohmic contacts. Hydrogen was reintroduced by etching the annealed samples in CP4A for 3–4 min. Schottky contacts were created by resistively evaporating Au (for n-type) or Al (for p-type) through a shadow mask onto the polished surface of the samples. Ohmic contacts were established by applying a eutectic InGa alloy to the backside of the samples. The quality of these contacts was verified using current–voltage and capacitance–voltage (C–V) measurements at room temperature and 50 K. The C–V measurements were performed at 1 MHz. Conventional DLTS and Laplace DLTS techniques were utilized to analyze the defect properties. The peak labeling in this work corresponds to the maximum temperature of the DLTS peaks at an emission rate of 47 s^{-1} and briefly indicates the defect assignment. The peak intensities in DLTS or Laplace DLTS spectra are not directly comparable, as the lambda-layer varies with temperature and the doping concentration changes with depth, particularly in hydrogenated samples. The concentration depth profiles of the defect levels were obtained using Laplace DLTS with a double pulse technique, as outlined in Ref. 18. To determine concentrations, the λ-layer was considered.[19] The electric field was calculated from C–V measurements as described in Ref. 19.

III. RESULTS

Figure 1 shows DLTS spectra recorded in as-grown samples after their annealing at 500, 600, and 700 °C in n- and p-type Si. The spectra were measured on different samples; therefore, the intensity of the peaks cannot be directly compared. In n-type Si, a dominant peak close to 260 K was observed in all samples independent of the annealing temperature. It is noteworthy, however, that the maximum of this dominant peak shifted when comparing samples annealed at 500 °C with those annealed at higher temperatures. The origin of this shift is discussed below. Two additional peaks labeled as $E105_{Ag}$ and $E148_{Ag}$, along with some minor peaks were also detected at lower temperatures in samples annealed at 500 and 600 °C. These peaks, however, disappeared after annealing at 700 °C.

In p-type Si, five DLTS peaks were observed after annealing the samples at 500 °C. The peak $H170_{Ag}$ dominates the DLTS spectrum, whereas the intensity of $H83_{Ag}$, $H105_{Ag}$, and $H225_{Ag}$ is approximately three times lower. In addition to these peaks, a minor peak was also observed around 260 K. The intensities of the peaks decrease significantly after annealing at 700 °C, leaving only a dominant peak, Ag (0/+), around 160 K, along with a small peak, Ag (−/0), near 260 K.

The samples annealed at 700 °C were used to investigate the interaction between Ag and H. In these samples, only two dominant peaks, labeled as Ag (−/0) and Ag (0/+), were observed, allowing us to avoid interactions with other Ag-related defects introduced during growth. The interaction of Ag-related defects observed in either as-doped samples or samples annealed at 500 °C with hydrogen has already been investigated in Refs. 10 and 15.

Figure 2 shows DLTS spectra recorded in n- and p-type Si samples annealed at 700 °C and subsequently hydrogenated in CP4 A. In n-type Si four DLTS peaks Ag (−/0), $E106_{AgH}$, $E160_{AgH}$,

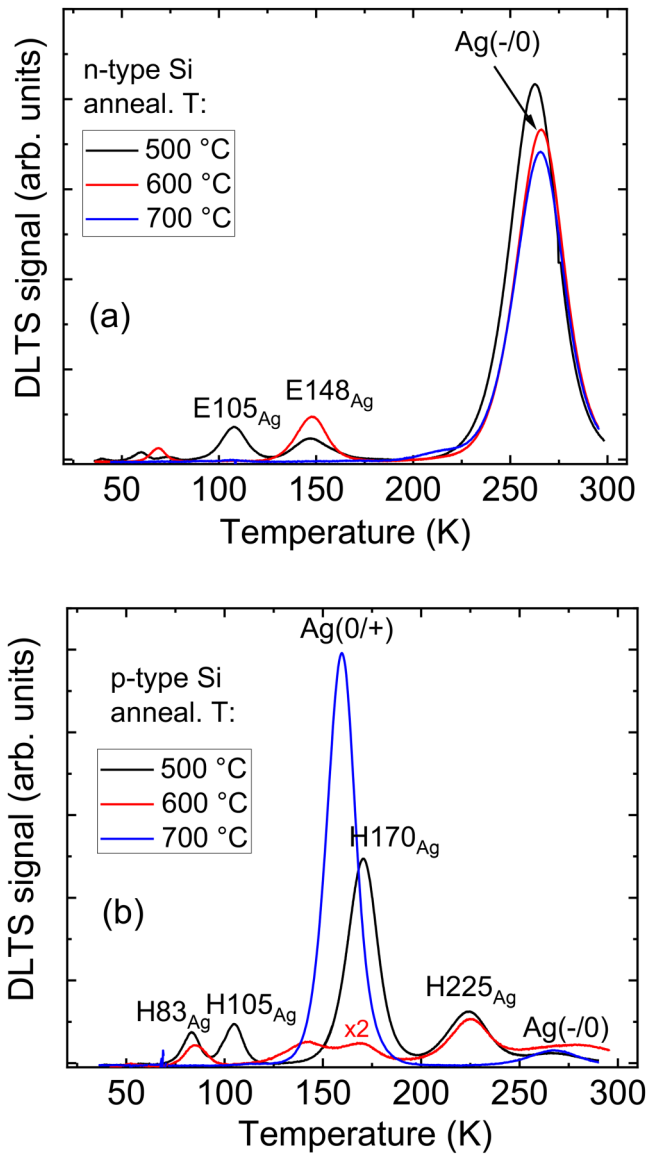

FIG. 1. DLTS spectra recorded from n-type (a) and p-type (b) samples after annealing at 500, 600, and 700 °C.

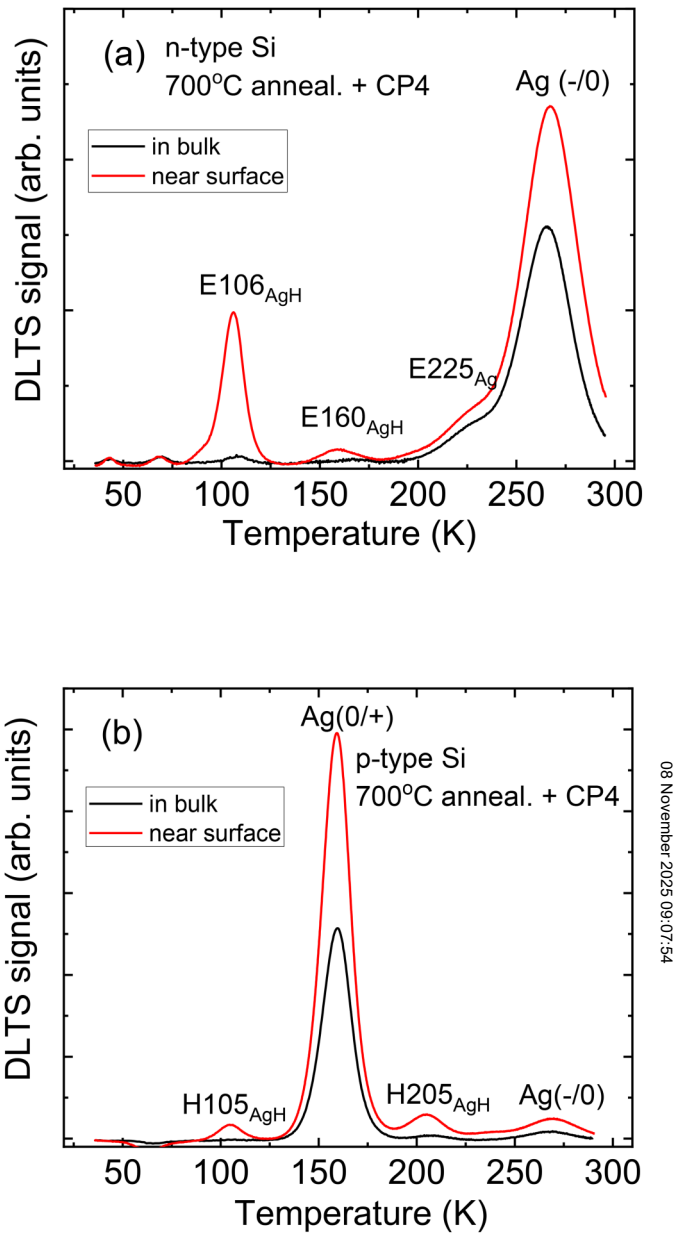

FIG. 2. DLTS spectra were recorded from n-type (a) and p-type (b) samples after annealing at 700 °C, followed by WCE. The spectra were measured using different filling pulses, both near the surface and deeper within the bulk.

and $E225_{Ag}$ as a shoulder to Ag (−/0) were observed near the surface in the annealed, hydrogenated samples. At greater depths within the bulk, the intensities of $E106_{AgH}$ and $E160_{AgH}$ decrease significantly, resulting in a substantial increase in the intensity ratio between Ag (−/0) and these peaks. In contrast, $E225_{Ag}$ was detected both near the surface and deeper in the bulk, with its intensity remaining approximately constant or even increasing relative to that of Ag (−/0).

In p-type Si, the Ag (0/+) peak remains dominant both near the surface and deeper in the bulk after hydrogenation of the annealed samples. In addition to this peak, $H105_{AgH}$ and $H205_{AgH}$ (with similar intensities), and Ag (−/0) were detected in hydrogenated p-type Si. However, the intensities of $H105_{AgH}$ and $H205_{AgH}$ decrease significantly when measured deeper in the bulk. In contrast, the intensity of Ag (−/0) scales similarly to Ag (0/+) at different measurement depths. To determine the depth profiles of these

defects and estimate their electrical properties, the high-resolution Laplace DLTS technique was employed.

Figure 3 shows Laplace DLTS spectra recorded at different temperatures in hydrogenated p-type Si samples. Two Laplace DLTS peaks, $H105_{AgH}$ and $H106_{AgH}$ appear at 115 K [Fig. 3(a)]. Notably, the intensity of $H105_{AgH}$ was three to four times larger than that of $H106_{AgH}$, depending on the measurement conditions.

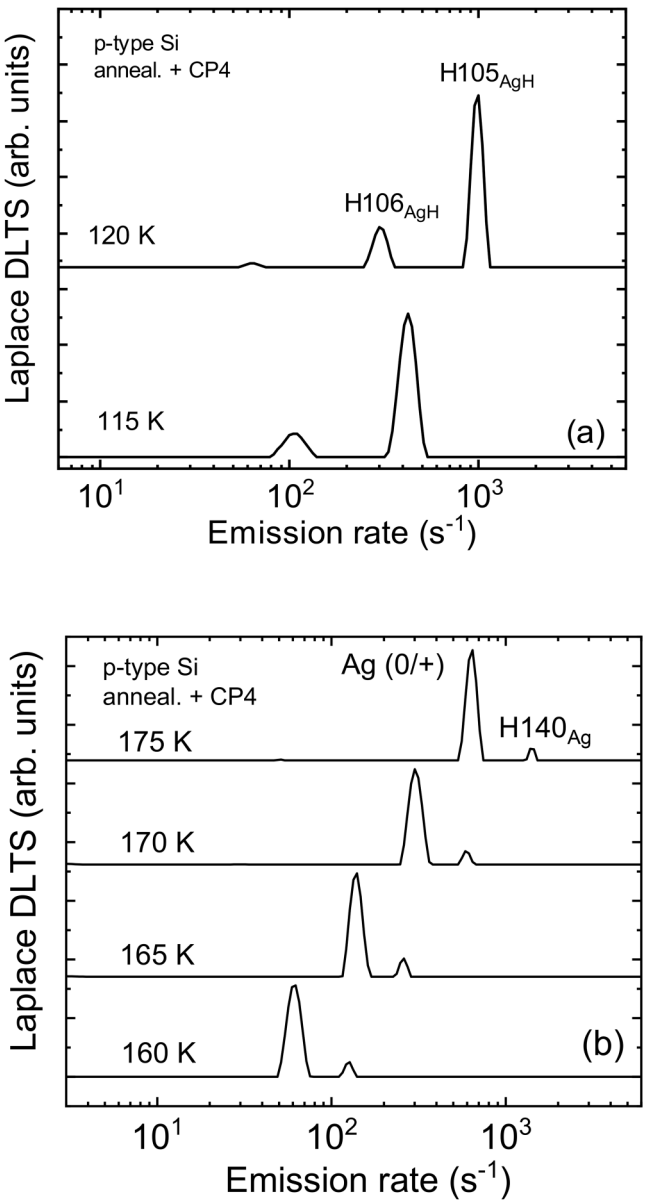

FIG. 3. Laplace DLTS spectra recorded from p-type samples after annealing at 700 °C, followed by WCE. Spectra shown in (a) and (b) were recorded at different measurement temperatures.

Two additional Laplace DLTS peaks, Ag (0/+) and $H140_{Ag}$ were also detected at 160 K in the same sample [Fig. 3(b)]. However, the intensities of $H106_{AgH}$ and $H140_{Ag}$ were only 1.5–2 times larger than the noise level, making the analysis of the electrical properties of these defects nearly impossible, even by using a large number of transients for the reduction of the level of noise. At 205 K, only a single Laplace DLTS peak, labeled as $H205_{AgH}$, was observed.

In hydrogenated n-type Si, single Laplace DLTS peaks, $E106_{AgH}$ and $E160_{AgH}$, were observed at 105 and 160 K, respectively, while three Laplace DLTS peaks Ag (−/0), $E225_{Ag}$, and $E265_{AgH}$ were resolved at 265 K (Fig. 4). By varying the voltage of two filling pulses while keeping the reverse bias applied to the diode constant, we observed a significant change in the ratio between the intensities of Ag (−/0) and $E265_{AgH}$. Near the surface, the intensities of $E265_{AgH}$ and Ag (−/0) are comparable, whereas Ag (−/0) becomes dominant in the bulk of the Si. The ratio between Ag (−/0) and $E225_{Ag}$ remains approximately constant, both near the surface and deeper in the bulk. We also note that the emission rate of the defects observed in Fig. 4 does not change significantly with variations in the voltage of the filling pulses.

Figure 5 shows the Arrhenius plots derived from the shift in the emission rates of the defects at different temperatures. The activation enthalpy and the apparent capture cross section of the defects, obtained from the Arrhenius plots, are summarized in Table I. We note that the activation enthalpy of the defect corresponding to the dominant DLTS peak in the sample annealed at

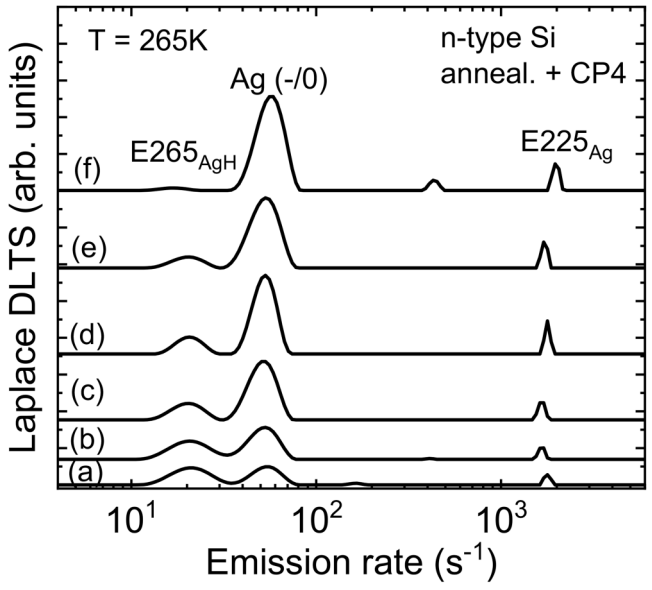

FIG. 4. Laplace DLTS spectra recorded from n-type samples after annealing at 700 °C and subsequent WCE at different temperatures. The spectra were measured with $V_R = -8$ V and the following pulse voltages: (a) $V_{p1} = -1$ V, $V_{p2} = -1.5$ V; (b) $V_{p1} = -1.5$ V, $V_{p2} = -2$ V; (c) $V_{p1} = -2.5$ V, $V_{p2} = -3$ V; (d) $V_{p1} = -3$ V, $V_{p2} = -3.5$ V; (e) $V_{p1} = -3.5$ V, $V_{p2} = -4$ V; and (f) $V_{p1} = -6.5$ V, $V_{p2} = -7$ V.

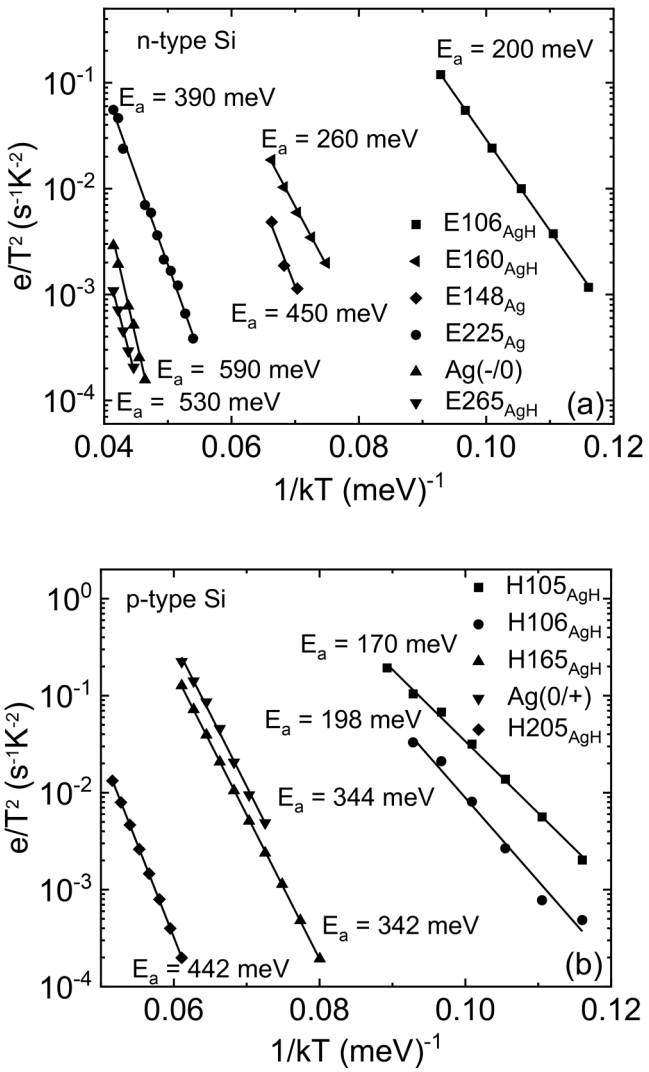

FIG. 5. Arrhenius plots of the traps observed in Figs. 1–4. The activation enthalpy is given in meV below the conduction band [n-type Si (a)] and above the valence band [p-type Si (b)].

500 °C is E_C−0.55 eV, which is lower than the value observed around 260 K in the sample annealed at 700 °C.

Figure 6 compares the depth profiles calculated from Laplace DLTS measurements with two filling pulses for the defects observed in Figs. 1–4 in hydrogenated n- and p-type Si. Phosphorous–hydrogen and boron–hydrogen profiles, obtained by subtracting the net free carrier concentration in the hydrogenated sample from the original concentration before hydrogenation, are also shown in this figure. Solid lines represent the fits to the experimental data (excluding points close to the surface) for defects with descending depth profiles toward the bulk. By analyzing the slope of the concentration reduction of the defects, we note that the concentrations of $E106_{AgH}$, $E160_{AgH}$, and PH decrease with an identical slope toward the bulk, while that of $E265_{AgH}$ is 2.1 times steeper. The depth profiles of $E148_{Ag}$, $E225_{Ag}$, and Ag (−/0) also decrease but toward the surface, reaching a maximum concentration at approximately 6–8 μm in the bulk of Si.

In p-type Si, identical depth profiles were obtained for $H105_{AgH}$ and $H205_{AgH}$, and the concentration of these defects decreased with the same slope as BH. Similar to Ag (−/0), the concentration of Ag (0/+) increases toward the bulk, reaching a maximum value of about 5×10^{13} cm^{-3} at around 8 μm.

The charge state of defects can be unambiguously determined only for defects with Coulomb potential by analyzing the changes in their emission rates as a function of the electric field. In this case, a linear dependence of the logarithm of the emission rate (e_n) on the square root of the electric field (E) should be observed. However, no such dependence of the emission rates on the electric field was observed for any of the defects shown in Figs. 1–3 in our samples.

TABLE I. Electrical properties of Ag and AgH-related defects observed in this study. The activation enthalpy and the apparent capture cross section σ_{na} were determined by Laplace DLTS from the Arrhenius plot [ln (emission rate/T^2 vs 1/T)].

Labeling of energy levels	Activation enthalpy (eV)	Apparent capture cross section (this work) (cm^2)	Capture cross section from the literature (cm^2)	Level identification
Ag (−/0)	E_C −0.59	4×10^{-14}	1×10^{-16}[11,14]	Ag (−/0)
Ag (0/+)	E_V + 0.344	8×10^{-14}	3×10^{-15}[12] 1×10^{-15}[11]	Ag (0/+)
$E106_{AgH}$	E_C −0.2	2×10^{-15}	1×10^{-17}[11]	AgH_1 (−/−)
$E160_{AgH}$	E_C −0.26	5×10^{-16}	9×10^{-15}[12] 5×10^{-16}[11]	AgH-related (−/−)
$E225_{Ag}$	E_C −0.39	8×10^{-17}	4×10^{-15}[12] 2×10^{-15}[11]	Ag-related (−/−)
$E265_{AgH}$	E_C −0.53	5×10^{-16}	6×10^{-17}[14]	AgH_2 (−/−)
$H105_{AgH}$	E_V + 0.17	1×10^{-15}		AgH_1 (0/+)
$H205_{AgH}$	E_V + 0.442	4×10^{-14}		AgH_1 (−/0)

IV. DISCUSSION

After heat treatments at 500–700 °C, a single DLTS peak dominates the spectrum at around 160 K in p-type Si and at around 260 K in n-type Si contaminated with Ag. However, we note that the maximum of the peaks in samples annealed at 500 °C is shifted compared to that observed after annealing at 700 °C in both n- and p-type Si. These DLTS peaks were not detected in reference samples without Ag, so we correlate them with Ag-related defects. The variation in activation energies of the defects corresponding to the dominant DLTS peaks shown in Fig. 1 after annealing at 500 and 700 °C cannot be explained by an enhancement of the emission rate due to increasing electric field: no such enhancement was observed when investigating the electric field dependence of all

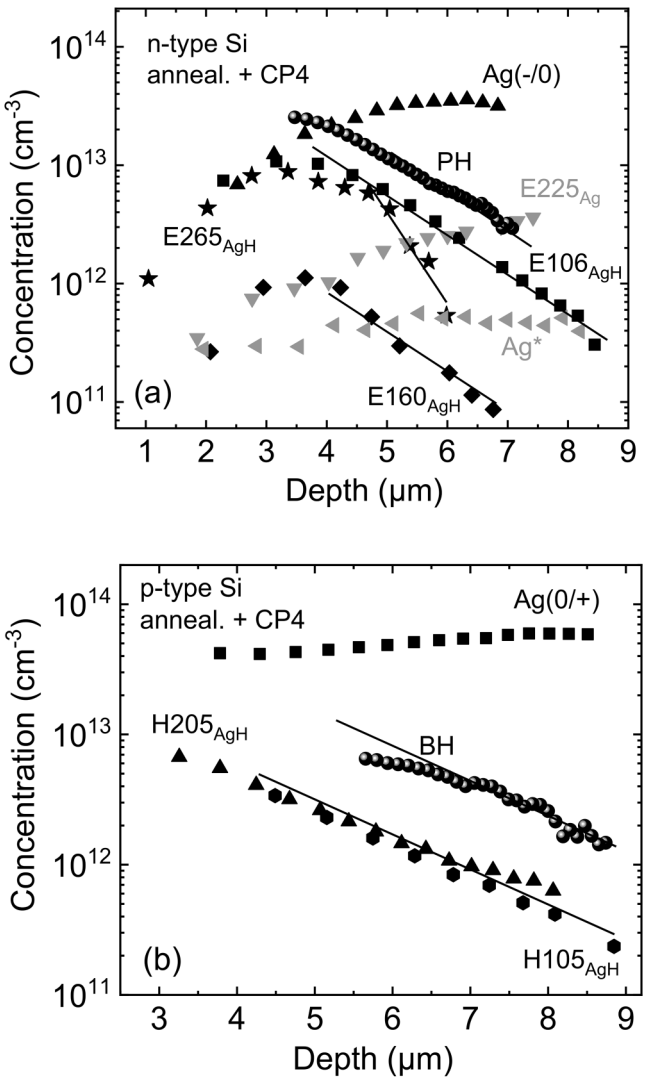

FIG. 6. Concentration depth profiles of defects observed in Figs. 1–4 after annealing at 700 °C, followed by WCE in n-type (a) and p-type Si (b). The solid lines are fits to the defect concentrations at larger depths.

defects presented in Figs. 1–3. Therefore, we assign the dominant Ag-related peaks observed after annealing at 500 and 700 °C to different defects. The differing origins of the dominant peaks in samples subjected to different heat treatments, and depending on the method of Ag introduction, could also explain the variation in the electrical properties of the defects assigned to Ag (−/0) and Ag (0/+) in the literature.[8–12]

Due to the absence of enhanced emission rates for any dominant defects with increasing electric field, we correlate them with acceptor- and donor-like defects in n- and p-type Si annealed at 700 °C, respectively. We also note that the concentration of Ag (−/0) and Ag (0/+) is similar (around 4–5 × 10^{13} cm^{-3}, as shown in Fig. 6) in the bulk of both n- and p-type Si annealed at 700 °C, supporting the idea of identical defect origins, especially considering the similar conditions of Ag introduction. Given the similar electrical properties of these defects to those of substitutional Au,[1–7] we tentatively attribute them to substitutional Ag as it is expected from both these impurities. The shift in the maximum of the dominant DLTS peaks in our samples annealed at 500 °C, compared to those observed after annealing at 700 °C, can be interpreted by the presence of unknown defects near Ag, which perturb the electrical properties of Ag_S, leading to a change in activation enthalpy. Similarly, the presence of Ge atoms in the vicinity of defects such as Fei, FeB, or CH in SiGe alloys with low Ge content (<3%) resulted in changes in the activation enthalpy of defects compared to defects without Ge.[20–23] We notice, however, that such an annealing step was necessary in the samples used in the present study, and it can be different depending on the doping and annealing conditions of Si samples.

Comparing the electrical properties of the small peak labeled as Ag (−/0) at around 260 K in p-type Si with those of the dominant defect Ag (−/0) in n-type Si we assign both of them to the same defect: the single acceptor state of substitutional Ag. The presence of Ag (−/0) in p-type Si can be interpreted by partial filling of this defect with electrons, which could be present at around RT.

We also observed a number of defects in both n- and p-type samples annealed at 700 °C and hydrogenated by WCE. These defects were not detected in the non-hydrogenated samples, and, therefore, we attribute them to H-related defects. Furthermore, we succeeded in separating $E265_{AgH}$ from Ag(−/0) for the first time using Laplace DLTS measurements. The descending profiles of $E106_{AgH}$, $E160_{AgH}$, and $E265_{AgH}$ in n-type Si, and $H105_{AgH}$ and $H205_{AgH}$ in p-type Si, are consistent with this assignment, as the concentration of H introduced by WCE also decreases from the surface to the bulk of Si. Feklisova and Yarykin[24] demonstrated that descending depth profiles of H-related defects after WCE can indicate the number of H atoms in the corresponding defects. According to their findings, the slope of the reduction in defect concentration for defects with the same number of H atoms should be identical, while it should be twice as steep for defects containing two H atoms. By comparing the depth profiles of $E106_{AgH}$ and $E160_{AgH}$ with that of PH, we assign these defects to complexes with one H atom in n-type Si, since the slope of the concentration reduction with depth is identical. In contrast, the slope of $E265_{AgH}$ is almost twice as steep as that of PH, indicating that it contains two H atoms. Similarly, $H105_{AgH}$ and $H205_{AgH}$ exhibit an identical slope to BH, suggesting that these defects contain one H atom in p-type Si.

If we sum the concentrations of $H105_{AgH}$, $H205_{AgH}$, and Ag (0/+) at different depths [Fig. 6(b)], we obtain a constant value of about 4–5 × 10^{13} cm^{-3} across the entire range in p-type Si. This observation further confirms that $H105_{AgH}$ and $H205_{AgH}$ are formed by the interaction of Ag (0/+) with H. In contrast, the sum of the concentrations of $E106_{AgH}$, $E265_{AgH}$, and $E160_{AgH}$ is smaller near the surface compared to the total concentration of Ag (−/0) in the bulk of Si [Fig. 6(a)]. This can be explained by the formation of electrically inactive AgH complexes close to the surface in hydrogenated samples. Previous studies have also reported the complete passivation of Ag-related acceptors in n-type Si using atomic H

plasma at 300 °C.[25] However, we note that the concentration of H introduced by WCE at room temperature is significantly lower compared to that in H plasma treatment at 300 °C. As a result, we were still able to observe the DLTS peaks associated with Ag even near the surface in hydrogenated n- and p-type Si, whereas these peaks were not visible after passivation with H plasma treatment.

The concentration of electrically inactive AgH complexes is also higher in n-type Si compared to p-type Si. We interpret this observation as a result of more effective interaction between Ag and H in n-type Si. Considering the doping levels of the n- and p-type Si samples used in this study, we calculated the position of the Fermi level to be around 220 meV below the conduction band in n-type Si and around 0.2 eV above the valence band in p-type Si. In this case, most of Ag should be negatively charged in n-type Si and positively charged in p-type Si. The charge state of H is also determined by the position of the Fermi level relative to the universal (+/−) level of H. The (+/−) level was calculated to be approximately 0.3 eV above the valence band,[26] while experimental values closer to the conduction band have been obtained through DLTS measurements (E_C−0.4 eV)[27,28] or muonium studies (E_C −0.34 eV) using muonium, a light isotope of H.[29,30] Therefore, the Fermi level in n-type Si should lie near the experimentally determined (+/−) level of H, while in p-type Si, it lies below this level. In this case, most of H should be positively charged in p-type Si and generally negatively charged in n-type Si. However, the close proximity of the Fermi level to the universal transition level of H could also result in a portion of H being positively charged in n-type Si. These H^+ ions could efficiently interact with negatively charged Ag^- and pre-existing AgH^- complexes, leading to the formation of more complex AgH defects. This interaction is less efficient in p-type Si due to the absence of Coulombic attraction between neutral or positively charged Ag and AgH complexes (the charge states of the defects are discussed below) and the positively charged H ions.

The electrical properties of the AgH-related levels observed in Figs. 1–4, along with their defect assignments, are summarized in Table I. Activation energies and apparent capture cross sections of these defects, as determined from Laplace DLTS measurements, provide a more precise characterization, particularly for defects with similar electrical properties that conventional DLTS cannot fully resolve. When varying the electric field, we did not observe any enhancement in the emission rate of AgH-related defects in either n- or p-type Si, suggesting these defects lack an attractive Coulomb potential. This behavior indicates that these defects likely act as acceptors in n-type Si or donors in p-type Si.

The capture cross sections of $E106_{AgH}$, $E160_{AgH}$, and $E265_{AgH}$ are smaller than that of Ag (−/0), leading us to assign these defects to double acceptor states. None of these defects exhibited a significant capture barrier, which might otherwise suppress emission rate enhancement in the presence of an electric field. In contrast, the capture cross section of $H105_{AgH}$ is comparable to that of Ag (0/+), suggesting it can be attributed to the single donor state in p-type Si. Meanwhile, the capture cross section of $H205_{AgH}$ is larger than that of $H105_{AgH}$. Since $H105_{AgH}$ and $H205_{AgH}$ represent different charge states of the same defect, and no evidence of a negative-U system was found, we assign $H205_{AgH}$ to the single acceptor state of AgH_1. Although this assignment is not unambiguous, it is consistent with the charge-state sequence and capture behavior previously reported for AuH-related levels in silicon.

Notably, previous studies have attributed different levels to the single donor and single acceptor states of AgH_1 and AgH_2. We also observed similar levels (E2, E3, E5, H2, and H3) in both n- and p-type Si that had been annealed at 500 °C and subsequently hydrogenated.[10] Consistent with Yarykin's findings, H2 and H3 were only detectable after reverse-bias annealing. The depth profiles of these defects closely match those reported in previous studies, confirming that E2, E3, and E5 are complexes with one H atom. However, the depth profiles of E2 and E3 were not identical as one expects from defects with the same origin. In addition, we did not detect these levels in our samples annealed at 700 °C. This contradicts to the assignment of E2 and E3 to the acceptors states of AgH. We also notice that, in our samples, the heating was switched off immediately after detaching the crystal after its growth and it was not constant. In contrast, Lemke[9] and Yarykin *et al.*[10] used n-type samples, which were cooled down at a constant rate of 1 or 10 K/s. The authors showed that even this difference in cooling rates leads to the appearance of different defects in the upper part of the bandgap of Si. This could also explain different Ag-related defects or different intensities of similar defects observed in the present study and in Ref. 10.

Figure 7 presents a schematic diagram of Ag-, AgH-, and AgH_2-related levels within the bandgap of hydrogenated Si. Our findings reveal strong alignment between the positions of levels in samples doped with Au and Ag, which also aligns with theoretical expectations. Given the structural similarity between substitutional Ag and Au, similar electrical properties are anticipated for AgH- and AuH-related complexes. At the moment, we cannot explain the difference of the charge state of AuH_2 and AgH_2. We notice

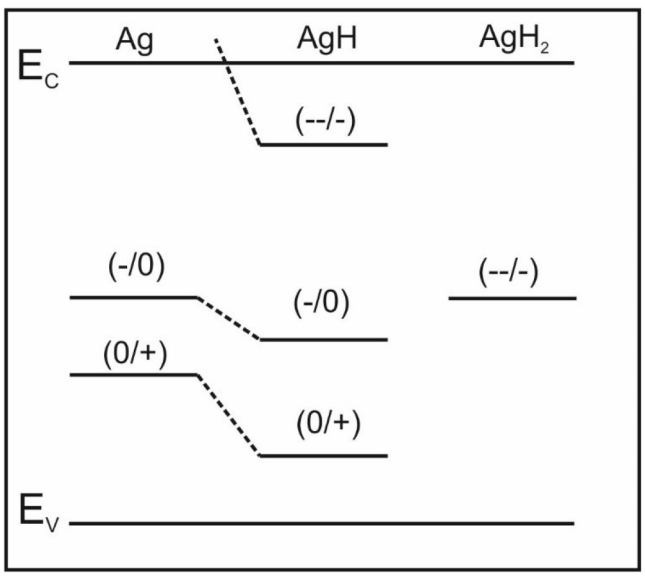

FIG. 7. Schematic diagram of Ag-, AgH- and AgH-related levels in the bandgap of hydrogenated Si.

however that the capture cross section of AuH_2 (−/0) is close to that observed for AgH_2 (–/−) and ,therefore, both defects could also possess the similar charge state.

V. SUMMARY

We correlated two DLTS levels with different charge states of substitutional Ag in samples annealed at 700 °C. In addition to these levels, another defect $E225_{Ag}$ that was not previously reported in the literature was also observed. The hydrogenation of the annealed samples leads to the appearance of different AgH-related defects ($E106_{AgH}$, $E160_{AgH}$, $E265_{AgH}$, $H105_{AgH}$, and $H205_{AgH}$), which were investigated in the present study. By analyzing the electrical properties and depth profiles of these defects, we showed that they were correlated with different charge states of AgH_1 ($E106_{AgH}$, $H105_{AgH}$, and $H205_{AgH}$) and the double acceptor state of AgH_2 ($E265_{AgH}$). We also tentatively correlated $E160_{AgH}$ with $E225_{Ag}$ after its interaction with H. In according to theory, we found a good correlation between the position of AgH-related defects and those observed in Au-doped Si.

ACKNOWLEDGMENTS

The authors thank Dr. Abrosimov and Dr. Lemke for supplying the samples with silver introduced during growth.

AUTHOR DECLARATIONS

Conflict of Interest

The authors have no conflicts to disclose.

Author Contributions

K. Gwozdz: Data curation (equal); Formal analysis (equal); Investigation (equal); Writing – review & editing (equal). **Vl. Kolkovsky:** Conceptualization (lead); Data curation (equal); Formal analysis (equal); Investigation (equal); Supervision (lead); Visualization (equal); Writing – original draft (lead); Writing – review & editing (equal).

DATA AVAILABILITY

The data that support the findings of this study are available from the corresponding author upon reasonable request.

REFERENCES

[1]C. B. Collins, R. O. Carlson, and C. J. Gallagher, Phys. Rev. **105**, 1168 (1957).
[2]A. F. Tasch and C. T. Sah, Phys. Rev. B **1**, 800 (1970).
[3]D. V. Lang, H. G. Grimmeiss, E. Meijer, and M. Jaros, Phys. Rev. B **22**, 3917 (1980).
[4]L.-Å. Lebedo and Z. G. Wang, Appl. Phys. Lett. **42**, 680 (1983).
[5]J. Utzig and W. Schröter, Appl. Phys. Lett. **45**, 761 (1984).
[6]J. W. Petersen and J. Nielsen, Appl. Phys. Lett. **56**, 1122 (1990).
[7]G. D. Watkins, M. Kleverman, A. Thilderkvist, and H. G. Grimmeiss, Phys. Rev. Lett. **67**, 1149 (1991).
[8]S. J. Pearton and A. J. Tavendale, J. Phys. C **17**, 6701 (1984).
[9]H. Lemke, Phys. Status Solidi A **94**, K55 (1986).
[10]N. Yarykin, J.-U. Sachse, H. Lemke, and J. Weber, Phys. Rev. B **59**, 5551 (1999).
[11]N. Baber, H. G. Grimmeiss, M. Kleverman, P. Omling, and M. Z. Iqbal, J. Appl. Phys. **62**, 2853 (1987).
[12]L. D. Yau and C. T. Sah, Appl. Phys. Lett. **21**, 157 (1972).
[13]A. Fazzio, M. J. Caldas, and A. Zunger, Phys. Rev. B **32**, 934 (1985).
[14]N. T. Son, V. E. Kustov, T. Gregorkiewicz, and C. A. J. Ammerlaan, Phys. Rev. B **46**, 4544 (1992).
[15]K. Gwozdz and Vl. Kolkovsky, Phys. Status Solidi A **218**, 2100217 (2021).
[16]A. Resende, R. Jones, S. Öberg, and P. R. Briddon, Phys. Rev. Lett. **82**, 2111 (1999).
[17]H. Feichtinger and E. Sturm, Mater. Sci. Forum **143–147**, 111 (1994).
[18]L. Dobaczewski, A. R. Peaker, and K. Bonde Nielsen, J. Appl. Phys. **96**, 4689 (2004).
[19]P. Blood and P. W. Orton, *The Electrical Characterization of Semiconductors Majority Carriers and Electron States* (Academic Press, 1992).
[20]R. Stübner, Vl. Kolkovsky, J. Weber, N. V. Abrosimov, C. M. Stanley, D. J. Backlund, and S. K. Estreicher, J. Appl. Phys. **127**, 045701 (2020).
[21]V. Kolkovsky, A. Mesli, L. Dobaczewski, N. V. Abrosimov, Z. R. Zytkiewicz, and A. R. Peaker, Phys. Rev. B **74**, 195204 (2006).
[22]V. Kolkovsky, A. Mesli, L. Dobaczewski, N. V. Abrosimov, Z. R. Zytkiewicz, and A. R. Peaker, J. Phys.: Condens. Matter **17**, S2267 (2005).
[23]R. Stübner, V. Kolkovsky, J. Weber, and N. V. Abrosimov, Phys. Status Solidi A **214**, 1700329 (2017).
[24]O. V. Feklisova and N. A. Yarykin, Semicond. Sci. Technol. **12**, 742 (1997).
[25]A. J. Tavendale and S. J. Pearton, J. Phys. C **16**, 1665 (1983).
[26]C. G. Van de Walle and J. Neugebauer, Nature **423**, 626 (2003).
[27]K. Bonde Nielsen, B. B. Nielsen, J. Hansen, E. Andersen, and J. U. Andersen, Phys. Rev. B **60**, 1716 (1999).
[28]K. B. Nielsen, L. Dobaczewski, S. Søgård, and B. B. Nielsen, Phys. Rev. B **65**, 075205 (2002).
[29]R. L. Lichti, K. H. Chow, and S. F. J. Cox, Phys. Rev. Lett. **101**, 136403 (2008).
[30]R. L. Lichti, H. N. Bani-Salameh, B. R. Carroll, K. H. Chow, B. Hitti, and S. R. Kreitzman, Phys. Rev. B **76**, 045221 (2007).